Developing asymmetries in AGB stars : occurrence, morphology and polarization of circumstellar Masers

Amiri, N.

5

The evolution of H_2O masers in the circumstellar environment of AGB stars in transition to Planetary Nebulae

N. Amiri, W. H. T. Vlemmings, H. J. van Langevelde
In preparation

Abstract

Observations have shown bipolar H_2O maser outflows in a class of post-AGB candidates, the so-called water fountain sources. Additionally, observations have established a significant correlation between the variability in flux density and profile shape with the stellar pulsation in Mira variables. However, it is not clear whether the H_2O masers exhibit similar variability behavior in higher mass loss AGB stars and in particular stars approaching the end of the AGB phase. The aim of this paper is to search for water-fountain sources in post-AGB candidates. A statistically relevant sample of these important transition objects is essential to study the evolution from spherically symmetric AGB stars to aspherical planetary nebulae. By observing in multi-epochs, we can also study the variability of the masers and compare them with those of Mira variables. We performed H_2O maser observations of a sample of 74 post-AGB candidates with the Effelsberg Telescope with a large velocity coverage ($\sim$1363 km s^{-1}). The observations were done at three epochs, spanning a timescale of $\sim$500 days. Additionally we observed the OH masers of the supposedly dead OH/IR star, IRAS 18455+0448, after we noticed the return of the H_2O masers, to check whether the OH masers are also back. We identified six water fountain candidates which show double peak profiles in at least one epoch. In particular, we detected the H_2O masers of a supposedly dead OH/IR star IRAS 18455+0448. Additionally, we found significant variability in flux density and spectral profile for the H_2O masers in our sample. Comparison of our observations with the observations of the same source sample performed $\sim$20 years ago by Engels & Lewis (1996) indicate the disappearance of 10 masers and the appearance of three new masers among a sample of 74 sources. Furthermore, the observations likely indicate a good correlation between the stellar pulsation and the H_2O maser variability. Furthermore, we estimate a lifetime of $\sim$60 years for the H_2O masers in the post-AGB phase. We identified potential water fountain candidates. Interferometric observations of the H_2O masers of these stars are essential to clarify this. In particular, if the bipolar scenario for the H_2O masers of IRAS 18455+0448 is confirmed, this star will be the youngest proto-PNe identified to date. Furthermore, the observations likely indicate a relation between the H_2O maser variability and pulsation cycle, as was previously found for Mira variables.

5.1 Introduction

The Asymptotic Giant Branch (AGB) phase is one of the last stages of stellar evolution for low to intermediate mass stars (1-8 $M_{\odot}$). At this stage, stars eject a significant amount of their mass into the interstellar medium in the form of stellar winds. The outflow from these objects forms Circumstellar Envelopes (CSEs) which harbor several molecular species. Among the best probes of evolved star mass-loss, outflow history and morphology are the masers that occur in different regions of the CSEs, as they probe the dynamics and kinematics of the outflow at various distances to the central stars. In the picture of regular AGB stars, SiO masers occur close to the central star (e.g. Cotton et al. 2008), while the H_2O and OH masers are found at progressively further distances (e.g. Habing 1996). The OH masers often exhibit double-peaked profiles with their velocities covering up to $\sim$ 25 km s^{-1} (e.g. te Lintel Hekkert et al. 1989), while the H_2O maser spectra are typically more irregular and have a velocity range confined within the OH maser spectrum (e.g. Bains et al. 2003).

Observations indicate that the majority of the observed PNe exhibit a range of complex morphologies (e.g. Balick et al. 1987), whereas their progenitor AGB stars are generally observed to be spherically symmetric. This implies that at some stage during the transition from the AGB phase to PNe, the spherically symmetric outflow changes to produce a-spherical PNe. A class of post-AGB objects have been discovered, which exhibit highly collimated H_2O maser jets (Likkel et al. 1992). The observed spectra and spatial distribution of these so-called water fountain sources are not consistent with those of regular AGB stars. The H_2O maser velocity range ($\sim$200 km s^{-1} or more) is much larger than the OH masers in these stars (e.g. Imai et al. 2008). Very Long Baseline Interferometry (VLBI) observations reveal collimated H_2O maser outflows in these stars (e.g. Imai et al. 2002, Boboltz & Marvel 2005). The dynamical ages of the water fountain jets studied at high-resolution range from few to a few hundred years, which has led to the conclusion that they represent a short transition phase between (post-)AGB and PN phase (Boboltz & Marvel 2007). The bipolar jets observed in water fountain sources are expected to be one of the major factors in shaping PNe, based on the existence of a large number of PNe with bipolar or multipolar morphologies (Sahai & Trauger 1998). This could indicate that during the post-AGB phase the jets carve out the CSEs and leave an imprint which manifests itself as asymmetric PNe at the later stage in the AGB evolution.

At the same time, the circumstellar masers, in particular H_2O masers, exhibit significant variability in spectral shape and flux density. H_2O maser monitoring observations of a sample of Mira variables reveal that the variability of the masers is related to the pulsation of the central star as well as the changes in the physical conditions in the interstellar medium (Rudnitskii & Chuprikov 1990, Shintani et al. 2008). However, it is not clear how the intensity and spectral profile of the H_2O masers vary for higher mass loss OH/IR stars and AGB stars approaching the end of the AGB phase. OH/IR stars are the extension of Mira variables towards larger masses and longer periods (up to 2000 days) and the CSEs of these stars are expected to be denser and larger (e.g. Herman & Habing 1985a).

In this paper, we present multi-epoch H_2O maser observations of a sample of post-AGB candidates with the Effelsberg Telescope. The primary goal of the observations is to identify water fountain candidates. Due to their short lived transition between the AGB and proto-PNe phase, only a handful of water-fountain candidates have been identified (e.g. Imai et al. 2007). However, a statistically relevant sample is important for our studies of the transition from spherically symmetric circumstellar envelopes into elliptical or even bipolar shapes of PNe. Additionally, the observations enable us to explore the variability behavior of H_2O masers in higher mass loss AGB stars and post-AGB

objects and compare them with those of Mira variables.

5.2 Observations and Data Reduction

We selected a sample of 74 evolved stars which are likely late AGB or early post-AGB objects (Table 5.3). All of these objects were previously observed with the Effelsberg telescope in an attempt to detect their H_2O maser emission (Engels & Lewis 1996). The sources were selected based on their location in the IRAS (60-25)/(25-12) color-color diagram (Fig. 5.1). The properties of the stars located in each region are shown in Table 5.1. Sources located in the regions IIIa, IIIb, IV, V are likely post-AGB candidates that have thick circumstellar shells and are likely undergoing a transition into PNe.

41 sources in our sample are objects for which no H_2O maser emission was detected in the earlier Effelsberg observations (Engels & Lewis 1996). The limited ($\sim$ 80 km s^{-1}) velocity coverage of the observations at the time could have failed to detect water-fountains which show high velocity H_2O maser outflows. Alternatively, maser variability, insufficient sensitivity or jet masers that were yet to appear can explain the non-detections. H_2O masers were originally detected for the remaining 33 sources in our sample. Among them, we selected sources for which some of the H_2O maser components lie outside the OH maser range, making them water fountain candidates.

We performed 22.23508 GHz H_2O maser observations of the source sample with the Effelsberg telescope. The full width half maximum (FWHM) of the telescope is 40.2 arcsec at the maser frequency ($\sim$ 22 GHz). Using the FFT spectrometer with 16384 channels and a bandwidth of 100 MHz ($\sim$1363 km s^{-1}) centered at the stellar velocity, the resulting spectral resolution is 0.08 km s^{-1}. The velocity coverage is much larger than that obtained in the previous observations of the source sample by Engels & Lewis (1996) ($\sim$80 km s^{-1}), which potentially could have missed to detect high velocity H_2O masers of water fountain sources.

The observations were performed in three epochs : 12 and 13 November 2009, 22 and 23 March 2011 and 14 April 2011. For the first two epochs we used the 1.3 cm primary beam receiver in spectral line mode. The 1.3 cm secondary VLBI receiver was used for the third epoch observations. The observations were made in position switching mode with a cycle of 1 min, sufficient to compensate for atmospheric fluctuations. The observing time for each source was 8-16 min at epoch 1, 8 min at epoch 2 and 12-24 min at epoch 3. The total observing time for first, second and third epochs were 14, 11 and 18 hours, respectively. The rms noise for the first, second and third epochs corresponds to 0.02-0.18, 0.06 and 0.07-0.3 Jy, respectively.

Additionally, we performed OH maser observations of IRAS 18455+0448 at 1612, 1665 and 1667 MHz. The observations were performed with the Effelsberg telescope after we observed the return of the H_2O masers of this star, to check whether the OH masers are excited again. We used the 21/18 cm primary focus receiver. At the OH maser frequency the FWHM of the telescope corresponds to $\sim$470 arcsec. Mainline OH maser observations at 1665.4018 and 1667.359 were performed on 22 Feb 2010 with a bandwidth of 20 MHz and 16384 channels which provides a channel spacing of $\sim$0.2 km s^{-1}. The total on source observing time was 2 hr and 26 minutes. The observations of 1612 MHz masers were made on 27 March 2010 with a bandwidth of 100 MHz and 16384 channels which corresponds to a channel spacing of $\sim$1 km s^{-1}. The total on source observing time was 72 minutes. The rms noise in channels free of emission is $\sim$7 mJy, for both epochs.

Region	Characteristic of the star
I	Oxygen rich non variable stars without any CSE
II	Variable oxygen rich stars with young CSE
IIIa	Variable stars with more evolved CSE
IIIb	Variable oxygen rich stars with thick CSE
IV	Variable oxygen rich stars with very thick CSE
V	Planetary nebulae and stars with cool CSE
VIa	Non variable stars with cold dust at large distances, mainly carbon-rich AGB stars
VIb	Variable stars with hot dust close to the star and cold dust at larger distances
VII	Variable stars with more evolved CSEs
VIII	Different objects

Table 5.1 – The properties of the stars located in different regions of the IRAS (60-25)/(25-12) diagram (van der Veen & Habing 1988).

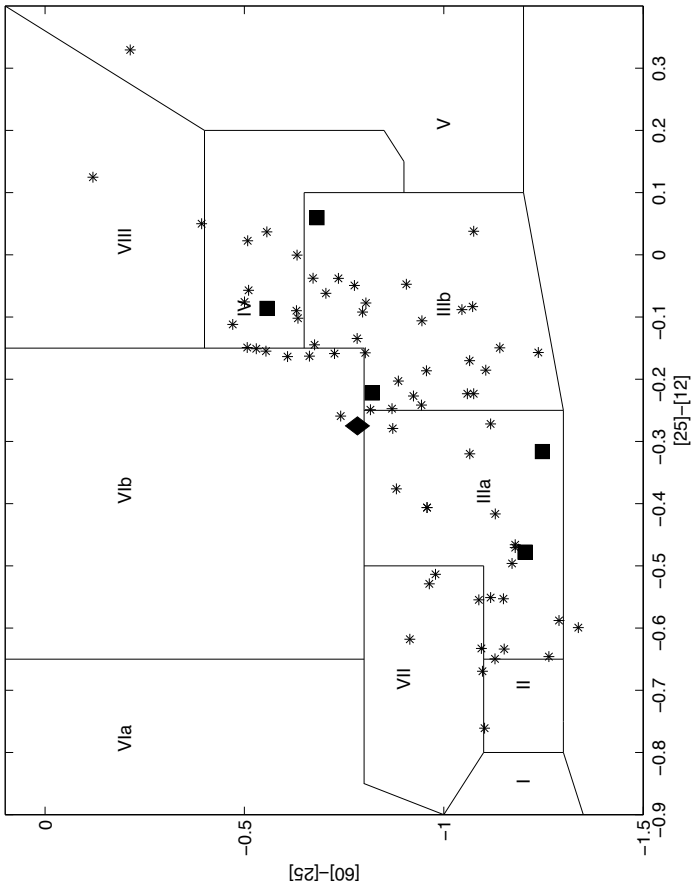

Figure 5.1 – Regions in the IRAS (60-25)/(25-12) color-color diagram which indicate various types of AGB stars (van der Veen & Habing 1988). The star symbols indicate the location of the sources in the diagram. The square symbols show the location of the water fountain candidates identified from the observations. The diamond indicates the location of the youngest proto-PNe candidate (IRAS 18455+0448).

The data reduction was performed using the Continuum and Line Analysis Single-dish Software (CLASS) package. The baseline for each spectrum was subtracted using the channels free of emission. From the observations, we obtained the raw spectra in units of temperature counts. The spectra were converted to units of antenna temperature (T_A) by applying the calibration noise temperature. We also corrected the spectra for atmospheric opacity and the gain-elevation effect. Finally, the spectra were converted to Jy units by dividing the spectra by the sensitivity of the telescope at the maser frequency.

5.3 Analysis

Table 5.4 shows the results of the observations. The spectra of the sources for which the H_2O masers were detected in at least one epoch are shown in Fig. 5.5-5.9. The analysis of the spectra observed at three epochs and comparison with the previous observations performed by Engels & Lewis (1996) reveal the appearance of new masers, the disappearance of some masers as well as significant variability in flux density and spectral shape. Among a sample of 74 sources observed, 10 masers have now disappeared. Additionally, we detected three new masers which were not observed to emit H_2O masers ∼20 years ago.

5.3.1 New masers

The observations indicate three stars which exhibit new H_2O masers (IRAS 18455+0448, IRAS 19012+0819 and IRAS 19254+1631). The masers were not detected in the earlier observations by Engels & Lewis (1996).

5.3.1.1 IRAS 18455+0448

We discovered the H_2O masers of IRAS 18455+0448. This object is considered as a prototype of a dead OH/IR star after a rapid disappearance of the 1612 MHz OH masers (Lewis et al. 2001). The 1612 MHz OH masers of this star were first observed by Chengalur et al. (1993), with a double peak profile at ∼27 and 40 km s^{-1} and a peak flux density of ∼2 Jy for the blue-shifted masers. Follow-up monitoring of the 1612 MHz OH masers of this star indicated exponential decay in flux density. The OH masers declined in flux density by up to a factor of 20, 12 years after the first detection of the masers (Lewis et al. 2001). Additionally, the peak intensity of the blue-shifted peak at 27 km s^{-1} of the 1665 MHz masers decreased linearly by a factor of ∼2 from 0.8 Jy in 1989 to ∼0.4 Jy in 2000. In the case of 1667 MHz masers, apart from flare like event in 1999, the blue shifted peak at 27 km s^{-1} also showed a decrease in flux density almost by a factor of ∼2 (1.6 Jy at 1998 and 0.7 Jy in 2000).

Fig. 5.5 shows the H_2O maser spectra of this star detected at three epochs with the Effelsberg telescope. The stellar velocity with respect to the local standard of rest (∼34 km s^{-1}) as well as the previously observed range for the 1612 MHz OH masers (∼27-40 km s^{-1}) are displayed in the figure. The spectrum shows emission blue-shifted with respect to the stellar velocity for the first two epochs with a peak flux density of ∼2 Jy. In the third epoch, the spectrum shows emission at ∼45 km s^{-1} with a peak flux of ∼1 Jy, red-shifted with respect to the stellar velocity. Interestingly,

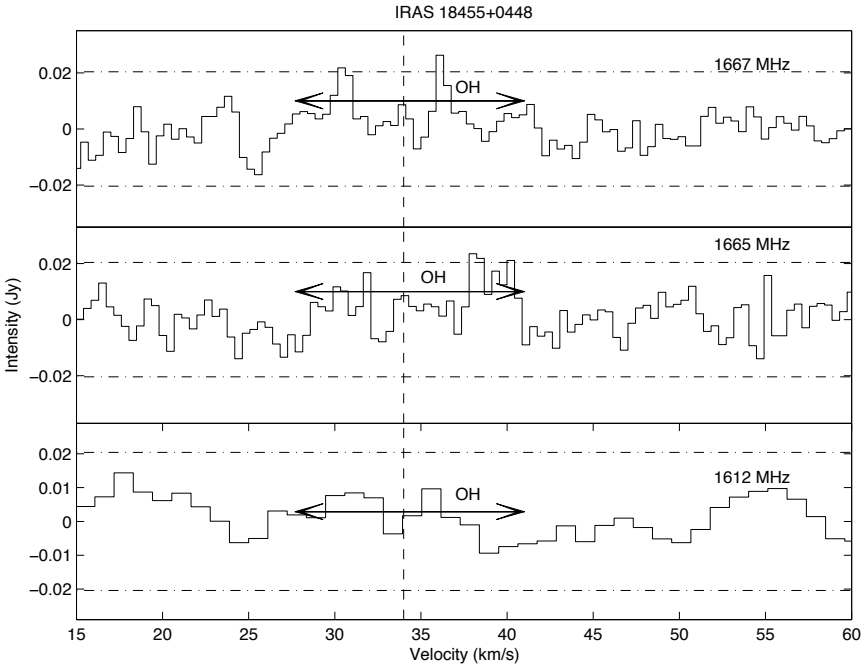

Figure 5.2 – The 1665 and 1667 MHz OH maser spectra of IRAS 18455+0448. The dashed-dotted horizontal lines are 3σ limits (~20 mJy). The vertical dashed line indicates the stellar velocity.

in all three epochs the H_2O maser emission range lies outside the 1612 MHz OH maser velocity range. This characteristic is not usually seen in the regular AGB stars.

We performed follow up observations of the OH masers of this star to check whether the OH masers are detectable again. Fig. 5.2 shows the OH maser spectra of IRAS 18455+0448 at 1612, 1665 and 1667 MHz. The observations indicate that the 1612 MHz OH masers have not reappeared together with the H_2O masers. Additionally, the observations show only a tentative detection at 1665 and 1667 MHz at 0.025 and 0.022 Jy, respectively. At both frequencies, the observed flux implies an order of magnitude decrease in flux density compared to the observations in 2000 by Lewis et al. (2001). We note that the peaks are at slightly different velocity compared to previously observed at these frequencies.

Engels & Lewis (1996) previously reported the absence of H_2O masers in this source. The appearance of the H_2O masers outside the OH maser velocity range, together with the non-detections of the 1612 MHz OH masers, raises the possibility that this object is in transition to become a PN. In particular the fact that the H_2O maser emission lies outside the OH maser velocity range, could indicate that a bipolar outflow is launched in this star. In order to reveal the nature of H_2O maser emission, follow up interferometric observations of the H_2O masers of this star, as well as monitoring observations at all transitions, are required.

5.3.1.2 IRAS 19112+0819

Fig. 5.7 shows the H_2O maser spectra of this star obtained at three epochs. The stellar velocity (V_{lsr} ~36 km s^{-1}) as well as the velocity range of OH maser emission are also shown in the figure.The masers were not detected in the first epoch. However, the maser profile shows the striking double peak profile in the second and third epochs. The maser emission is detected at ~21.6 and ~54 km s^{-1} with a peak flux density of ~2 Jy for the red-shifted complex. Comparison of the OH and H_2O maser velocity range in the second and third epochs shows a similar velocity range for both maser transitions.

5.3.1.3 IRAS 19254+1631

The H_2O maser spectra of this source observed at three epochs are shown in Fig. 5.7. In all epochs, the spectra show three emission complexes red-shifted with respect to the stellar velocity (1.9 km s^{-1}). The range of OH maser emission is also shown in the figure.

5.3.2 Variability of the H_2O masers with respect to stellar pulsation cycle

Our multi-epoch observations which spans over a time scale of ~500 days, enable us to study the possible relation between the variability behavior of H_2O masers with respect to the stellar pulsation cycle. We detected the H_2O masers of 23 sources in the first epoch. Among these sources, four stars lost the masers in the second and third epochs: IRAS 19081+0322, IRAS 19425+3323, IRAS 19565+3140 and IRAS 20267+2105. We define the short time scale variability for H_2O masers in the post-AGB phase. We assume that the variability time scale of the H_2O masers is 'T' days. The probability that 'm' H_2O masers have disappeared after a re-visit of Δt days among a sample of 'n' masers can be calculated according to the law of combinatorics (Engels & Jiménez-Esteban 2007):

$$P_n^m = \frac{n!}{m!\,(n-m)!} \times \left(\frac{\Delta t}{T}\right)^m \times \left(1 - \frac{\Delta t}{T}\right)^{n-m} \tag{5.1}$$

The 'n' and m values in Eq. 5.1 correspond to 23 and 4, respectively. Fig. 5.3, shows the probability of the disappearance of 3 maser features in the second epoch (Δt ~ 485 days). The figure shows a variability time scale of ~3000 days (~8 years) for the H_2O masers in the post-AGB phase. We note that the estimated variability timescale is similar to the period of high mass loss OH/IR stars (~2000 days more more). This indicates similar variability properties for OH/IR stars exist, which implies the variability of the masers are related to the pulsation period as was previously found for Mira variables (Shintani et al. 2008).

5.3.3 Disappearing H_2O masers

The observations also enable us to study the longer time scale variability by comparing the observations to the original work by Engels & Lewis (1996). The source sample includes 33 H_2O masers which were detected by Engels & Lewis (1996). We found that 10 sources no longer exhibit maser

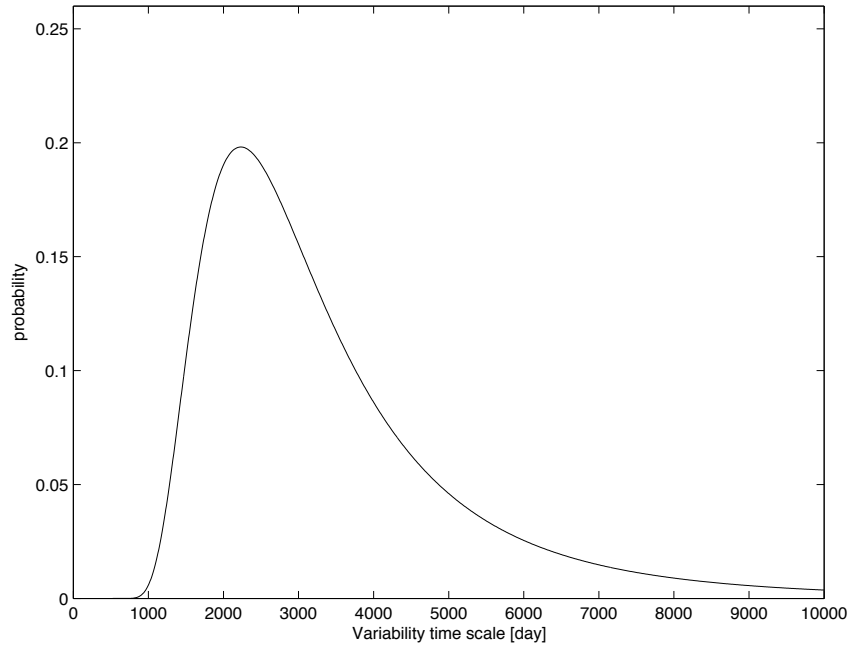

Figure 5.3 – Probability (P_n^m), that m=4 masers have disappeared among a sample of n=23 masers detected in the first epoch of our observations. The horizontal axis indicates the variability time scale (T) of the H_2O maser features in days.

emission in our multi-epoch observations. Table 5.2 lists the H_2O masers which were observed to have H_2O masers ∼20 years ago, but no longer show maser emission. The 3σ upper limit for flux density is also given for every source at each epoch. We assume that AGB stars only support maser emission at specific times since the masers require optimal coherence path. If the stars which no longer exhibit maser emission in our multi-epoch observations do not come back, we can estimate the lifetime of the masers statistically according to Eq. 5.1. We assume that the lifetime of the H_2O masers is 'T' years. The 'm' and 'n' values from our observations correspond to 10 and 33, respectively. Fig. 5.4 displays the probability of finding 10 masers disappeared after a re-visit of 20 years. The figure shows a lifetime of ∼60 years for H_2O masers in the post-AGB phase.

However, the overall lifetime of the H_2O masers is the lower limit. As mentioned in previous section, H_2O masers exhibit short time scale variability which is likely related to the stellar pulsation. This could imply that the disappearance of the masers could be the related to the stellar pulsation and that the masers may come back again at a later time. This is already evident as we have seen three masers return from previous observations ∼20 years ago. As the sources selected from the detections and non-detections sample are of similar sizes, this could imply that three masers could return at a later time among the 10 masers disappeared. In that case the value of 'm' in Eq. 5.1 changes. For illustration, we show in Fig. 5.4 curves with m=10, 7 and 3 which indicate the result of over estimate of the disappeared masers. Therefore, the overall lifetime of the H_2O masers in the post-AGB phase could be much longer.

Additionally, the estimated lifetime of the masers may be influenced by the sensitivity limitations of the telescope. Therefore, it is possible that the star still exhibits maser emission, but the maser intensity is below the sensitivity of the telescope.

5.3.4 Individual Sources with double peak profiles

Water fountain sources are defined by having high velocity H_2O maser outflows (e.g. Likkel et al. 1992). The H_2O maser velocity is typically larger than the OH maser velocity range traced by 1612 MHz OH maser observations (10-20 km s^{-1}, te Lintel Hekkert et al. 1989). From the Effelsberg observations, we identified several water fountain candidates which exhibit the striking double peak profiles in at least one observation epoch. We note that the velocity extent of the sources identified is not as large as those observed previously for other water fountain sources (e.g. ∼200 km s^{-1}, Imai et al. 2008).

5.3.4.1 IRAS 19422+3506

We detected a double peak profile together with emission close to the stellar velocity for IRAS 19422+3506 (Fig. 5.7). The stellar velocity with respect to the local standard of rest (-48.4 km s^{-1}) as well as the range of the OH maser emission are also shown in the figure. Previous H_2O maser observations of this star indicated a single peak profile at −60.9 km s^{-1} with a peak flux density of 52 Jy (Engels & Lewis 1996). Shintani et al. (2008) also observed the H_2O maser of this star, but no detection was reported.

The H_2O maser spectrum of this source at the first epoch (Fig. 5.7) shows double peak structure at -40 and -70 km s^{-1}. Also, there are central peaks close to the stellar velocity (-48 km s^{-1}). The double peak structure could indicate that the maser emission originates in a jet that lies close to

source	V_p km s^{-1}	Flux Jy	3σ (epoch 1) Jy	3σ (epoch 2) Jy	3σ (epoch 3) Jy
IRAS 18341+0005	57.7	0.2	0.3	0.4	0.4
	59.6	0.6			
IRAS 18568+0550	-50	0.2	0.3	0.5	0.4
IRAS 18578+0831	36.8	0.3	0.35	0.3	0.4
IRAS 19017+0412	98.6	2.4	0.14	0.3	0.7
IRAS 19043+1009	34.8	2.6	0.5	0.3	0.4
IRAS 19052+0922	37.8	0.4	0.35	0.3	0.4
	54.8	0.7			
IRAS 19054+0419	-51.1	0.45	0.35	0.3	0.4
	-48	0.4			
	-30.3	0.15			
IRAS 19316+0919	78.5	6.1	0.13	0.3	0.13
IRAS 19462+2232	4.5	7	0.55	0.2	0.9

Table 5.2 – H_2O masers which were detected in previous observations by Engels & Lewis (1996), but have now disappeared in our multi-epoch observations. The first column shows the velocity at which the masers were detected and the second column lists the observed flux densities of the masers in the original observations (Engels & Lewis 1996). The last three columns indicate our upper limits.

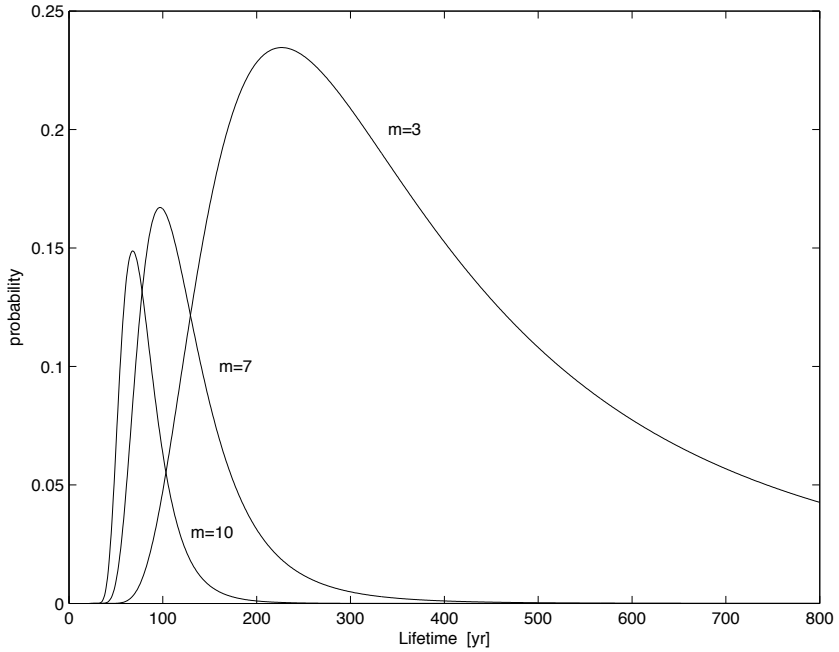

Figure 5.4 – Probability (P_n^m), that m=10, 7 and 3 masers have disappeared among a sample of n=33 previously detected H_2O masers. The horizontal axis indicates the lifetime T of the H_2O masers.

the plane of the sky, but it could also imply the radial amplification of the masers (Engels & Lewis 1996, Engels et al. 1997). The presence of the inner peaks could indicate that the inner peak masers occur in the equatorial plane of the circumstellar shell (Walsh et al. 2009).

Comparison of the H_2O maser spectra of this source obtained at three epochs shows significant variability in spectral shape and flux density. At the first epoch, the red-shifted peak was detected at ∼13 Jy. However, for the second and third epochs the flux density has decreased by about an order of magnitude. In the second epoch, the emission close to the stellar velocity has the highest flux density (∼1 Jy). At the third epoch which was performed about three weeks apart from the second epoch observations, the spectral shape is similar to that observed in the first epoch and the red-shifted emission has a flux density of ∼1.3 Jy. Similar phenomena are known from monitoring observations of the H_2O masers of the OH/IR star OH 39.7+1.5, which showed evidence of mode switching between radial and tangential amplification with the stellar pulsation cycle (Engels et al. 1997). This star has a period of ∼1430 days (Van Langevelde et al. 1990). During the stellar maximum the maser profile was similar to the double peak OH maser profile which indicates the radial amplification of the masers. However, close to the minimum phase of the stellar pulsation which occurred ∼550 days after the stellar maximum, the radially beamed masers disappeared and the profile only showed emission close to the stellar velocity which implies the masers are tangentially amplified. Engels et al. (1997) argue that both the tangential and radially beamed masers are located in the same region and that due to the competitive gain, tangential amplification occurs only when the physical conditions are not sufficient to excite the radially beamed masers.

Therefore, the mode switching between the radial and tangential amplification of IRAS 19422+3506 could be related to the stellar pulsation. Monitoring H_2O maser observations of this star over a longer timescale is required to clarify the variability of the maser profile with respect to the stellar pulsation cycle.

5.3.4.2 IRAS 19067+0811

The H_2O masers of this star were not detected at the first epoch (Fig. 5.6). However, in the second and third epochs we observed a double peak profile at 45 and 78 km s^{-1} with a peak flux density of 3.5 Jy for the red-shifted complex of the H_2O masers of this star. The stellar velocity (59.2 km s^{-1}) as well as the range of OH maser emission are also shown in the figure. Previous observations of this star by Engels & Lewis (1996) only indicated a single peak profile for the red-shifted emission with a peak flux density of 3 Jy.

5.3.4.3 IRAS 19069+0916

We observed a double peak profile for the H_2O masers of this star at the first epoch at ∼13 and 46 km s^{-1} with a maximum flux density of ∼7 Jy for the blue-shifted complex (Fig. 5.6). For the second and third epochs the spectra only show a single peak at ∼18 km s^{-1} with a flux density of ∼0.8 Jy. The stellar velocity (32.7 km s^{-1}) as well as the range of OH maser emission are also shown in the figure. Previous observations of this star also showed double peak profiles at ∼11 and 44 km s^{-1}, with a peak flux density of 2.4 and 0.4 Jy, respectively.

5.3.4.4 IRAS 19186+0315

The H_2O maser spectrum of this star shows a double peak profile at -35 and -15 km s^{-1} in all three epochs (Fig. 5.7). The blue shifted component has the higher flux density in each epoch. We note that the spectral shape appears consistent during our multi-epoch observations. However, the previous observations of the H_2O masers of this star only showed emission at -33.7 km s^{-1} with a flux density of 6 Jy (Engels & Lewis 1996).

5.4 Discussion

5.4.1 Water Fountain Candidates

As mentioned earlier, water fountain sources often show high velocity H_2O maser outflows (e.g.~200 km s^{-1} or more, Likkel et al. 1992, Imai et al. 2008). From our multi-epoch observations, we identified six water-fountain candidates : IRAS 18455+0448, IRAS 19112+08129, IRAS 19422+3506, IRAS 19067+0811, IRAS 19069+0916, and IRAS 19186+0315. The locations of these sources in the IRAS (60-25)/(25-12) color-color diagram are shown in Fig. 5.1. The H_2O maser spectrum of all these stars exhibits a double peak profile at least in one epoch. The double peak profile raises the possibility that a bipolar outflow is launched in these stars.

However, the water-fountain candidates that we identified, do not exhibit a large velocity extent in their H_2O maser profile. One possibility is that the projection of the velocity vector along the line of sight for a jet in the plane of the sky results in a V_{lsr} maser velocity range that is not as wide. Additionally, the lower velocity extent could indicate that the masers are located in biconical outflows, which do not necessarily exhibit a large velocity extent in the spectrum (Maeda et al. 2008). Alternatively, this could imply that the jet is recently launched and is accelerating outwards. Previously, water fountains with lower velocity outflows for H_2O masers have been reported. For example, the H_2O maser jet of the water fountain source, OH 12.8-0.8, only shows ~55 km s^{-1} velocity extent (Boboltz & Marvel 2005). Additionally, the interferometric observations of the OH maser region of this star showed that the H_2O maser jet lies inside the OH maser shell which implies that the jet could be recently launched in this star (Amiri et al. 2011). In order to clarify this, interferometric observations of the H_2O masers of these stars are required to obtain the spatial distribution of the H_2O masers.

Alternatively, the double peak profile observed for the H_2O masers may indicate radial amplification of the H_2O masers. Engels & Lewis (1996) divide the H_2O maser spectra of evolved stars into two groups. Group A sources show emission close to the radial velocity of the star, as commonly observed for Mira variables. The H_2O masers in this case are located close to the central AGB star. At such distances there is large velocity gradient along the radial direction and as a result the masers are tangentially amplified. However, sources in group B display double peak profiles with velocities close to those of OH masers. High mass loss rate OH/IR stars likely belong to this group. The H_2O maser shell is located at larger distances compared to the location of H_2O masers in lower mass loss rate Mira variables. At such large distances, there is lower velocity gradient which allows the radial amplification of masers, that manifest itself in double peak profile. This type of profile is usually observed for high mass loss OH/IR stars. Moreover, in one of our objects, IRAS 19422+3506, we found confirmation of the model proposed by Engels et al. (1997) for the changes in the H_2O maser

emission in the OH/IR star OH 39.7+1.5. It seems possible that in some OH/IR stars the maser amplification switches from radial to tangential within the stellar pulsation.

5.4.2 IRAS 18455+0448, Youngest proto-PNe candidate

We discovered the H_2O masers of the supposedly dead OH/IR star IRAS 18455+0448. The exponential decline of the 1612 MHz OH masers of this star were previously reported by Lewis et al. (2001). The lack of the OH masers could imply that the mass-loss has stopped in this star. Interestingly, our followup observations of the OH masers (1612, 1665 and 1667 MHz) indicate that this star seems to emit weak mainline masers, but not the 1612 MHz OH masers. This could be due to the fact that the 1612 MHz masers require larger column density and as a result of the cessation of the mass-loss, they disappear faster than the mainline masers (Lewis 1989).

The detection of the H_2O masers in this source could have two explanations. First possibility is that the mass loss has resumed in this star and that the H_2O masers are emitted close to the central star. The other possibility would be that the H_2O masers are excited in the wind, outside the OH masers at the tips of a jet. In particular, we found that the H_2O maser velocity range is larger than the previously observed 1612 MHz OH maser emission (Fig. 5.5), which is an essential characteristic of water-fountain sources. To clarify between these two possibilities, we need high resolution interferometric observations to obtain the spatial extent of the H_2O masers and accurate positions for follow up VLBI observations. In particular, if the second scenario (jet) is confirmed, this source will be the youngest proto-PN identified so far.

5.4.3 Variability

We observed a sample of 74 post-AGB candidates to monitor the variability of the H_2O masers in the pre-PNe stage. The sources in our sample are mainly OH/IR stars which are expected to have thicker and denser circumstellar shells compared to Mira variables. OH/IR stars are expected to have longer periods, ~2000 days or more. The multi-epoch observations covered a time scale of ~500 days. We found that the H_2O masers exhibit significant variability in flux density and spectral characteristics. We observed the rise of new maser features that differ by as much as 35 km s^{-1} in velocity from features detected in the earlier observations (e.g. IRAS 19422+3506; Fig. 5.7). H_2O masers in regular AGB stars are located in a region where the medium is highly turbulent and undergoes radial acceleration. Rudnitskii & Chuprikov (1990) attribute the variability of the H_2O masers to the shock waves propagating in the H_2O maser region. These shock waves are periodically generated in the H_2O maser region and travel outward in the CSE. However, it is not clear how shock waves with a few km s^{-1} speed can have an strong effects in the H_2O maser zone.

H_2O maser monitoring in Mira variables with a time spacing of 1-2 months revealed good correlation between the stellar light curve and the H_2O maser emission (Shintani et al. 2008). Their results show that the H_2O maser emission changes over the pulsation cycle of the star. Since the sources studied in our work belong to a different class of AGB stars, we do not have optical light curves available to study the correlation between the stellar pulsation and the H_2O maser emission. However, our observations likely show a correlation between the stellar pulsation cycle and the short time scale variability (~3000 days, Fig. 5.3), which is the same order of magnitude as the pulsation of high mass loss OH/IR stars.

For 10 sources, we observed disappearance of the masers, compared to the earlier observations performed ~20 years ago by Engels & Lewis (1996). Assuming that the masers do not come back again, we estimate a lifetime of ~60 years for H_2O masers in the post-AGB phase from statistical arguments. Since our multi-epoch observations only cover a timescale of ~500 days, which is much shorter than the period of OH/IR stars (2000 days or more), we can not confirm that the masers will not rise up again. Therefore, follow up monitoring H_2O maser observations spanning the whole period of OH/IR stars are required to clarify this. Additionally, follow up 1612 MHz OH maser observations of the sources are required to understand whether the stars which already show a decline in the H_2O maser emission, still exhibit 1612 MHz OH maser emission. The lack of OH maser emission could imply limited lifetime of the masers in the post-AGB phase.

It is not clear however, whether stars only support maser emission once during the AGB and post-AGB phases or H_2O masers turn on and off several times. OH/IR stars are found to be dead when they no longer exhibit 1612 MHz OH maser emission (Lewis 2003, Lewis et al. 2001). A dead OH/IR star can then undergo one of the two evolutionary scenarios. In the first scenario the mass loss stops and the CSE expands sufficiently that it no longer exhibits maser emission. The star then first become a proto-PNe and finally a PN. Alternatively, the mass loss can decrease temporarily after a Helium shell flash, despite the fact the star is still in the AGB phase and maintains the CSE (Lewis et al. 2001). In this scenario, the masers will be back after the mass loss resumes. Monitoring observations of the 1612 MHz OH masers of a sample of OH/IR stars that showed decline in flux density indicated that most AGB stars likely go through an OH/IR phase several times during the AGB phase (Lewis 2003).

5.5 Conclusions

We performed 22 GHz multi-epoch observations of a sample of post-AGB candidates. We identified six water fountain candidates which exhibit the striking double peak profile in at least one epoch. The double peak profile is a strong indication that a bipolar H_2O maser outflow is launched in these stars. Follow up interferometric observations of the identified water fountain candidates are required to understand the spatial distribution of the H_2O masers. In particular, if a bipolar H_2O maser jet is confirmed for IRAS 18455+0448, this source could be the youngest proto-PNe candidate identified so far.

Furthermore, we found that the H_2O masers of the post-AGB candidates studied in this work, exhibit large variability in flux density and profile shape. We estimate an overall lifetime of ~60 years for the H_2O masers in the post-AGB phase. Additionally, the observations likely indicate that the variability on shorter timescale (~3000 days) is related to stellar pulsation, as was previously found for Mira variables.

Table 5.3 – Source sample

	IRAS Name	RA (J2000)	Dec (J2000)	[25-12]	[60-25]	V_{lsr} km s^{-1}
1	IRAS 18095+2704	18 11 30.67	+27 05 15.5	0.0381	-1.0752	-4.6
2	IRAS 18341+0005	18 36 40.67	+00 08 01.2	-0.5528	-1.1496	85.4
3	IRAS 18349+1023	18 37 19.26	+10 25 42.2	-0.7609	-1.1022	-32
4	IRAS 18353+0020	18 37 55.79	+00 23 31.6	-0.0831	-1.0722	-43.5
5	IRAS 18395+0130	18 42 03.10	+01 33 15.0	-0.1863	-0.9565	48.6
6	IRAS18398+1035	18 42 09.98	+10 38 54.9	-0.6327	-1.0944	78.6
7	IRAS 18455+0448	18 48 02.30	+04 51 30.5	-0.2748	-0.7835	34.1
8	IRAS 18475+0353	18 50 00.1	+03 56 32	-0.0568	-0.5105	25.8
9	IRAS 18490+0302	18 51 35.64	+03 05 55.9	-0.259	-0.7416	130.9
10	IRAS 18534+0215	18 55 59.0	+02 19 06	-0.1509	-0.53	39.6
11	IRAS 18549+0208	18 57 27.5	+02 12 16	-0.0757	-0.5003	77.9
12	IRAS 18549+0905	18 57 20.82	+09 09 40.9	-0.496	-1.1713	19.4
13	IRAS 18568+0550	18 59 20.74	+05 54 41.1	-0.1446	-0.6761	-52
14	IRAS 18571+0611	18 59 35.98	+06 15 36.6	-0.149	-0.5071	35.4
15	IRAS 18578+0831	19 00 17.5	+08 35 29	-0.2028	-0.886	48.8
16	IRAS 18596+0315	19 02 06.28	+03 20 16.3	0.3296	-0.2136	88.4
17	IRAS 19006+0624	19 03 03.3	+06 28 52	-0.1635	-0.6082	-31
18	IRAS 19012+1128	19 03 36.71	+11 33 03.4	-0.5509	-1.1173	53.7
19	IRAS 19017+0412	19 04 14.42	+04 16 59.5	-0.2718	-1.1176	85.8
20	IRAS 19017+0608	19 04 09.71	+06 13 16.0	-0.1344	-0.7826	148.6
21	IRAS 19035+0451	19 05 58.91	+04 55 45.6	-0.5134	-0.9794	88.9
22	IRAS 19043+1009	19 06 43.0	+10 14 32	-0.4164	-1.1292	49.5
23	IRAS 19052+0922	19 07 38.91	+09 27 16.6	-0.5288	-0.9636	44
24	IRAS 19054+0419	19 07 55.9	+04 23 51	-0.249	-0.8162	-37
25	IRAS 19065+0832	19 08 58.8	+08 37 45	-0.0003	-0.6322	53.1
26	IRAS 19067+0811	19 09 07.471	+08 16 22.52	0.0599	-0.682	59.2
27	IRAS19069+0916	19 09 19.4	+09 21 13	-0.086	-0.5568	31.8

Table 5.3 – Continued.

	IRAS Name	RA (J2000)	Dec (J2000)	[25-12]	[60-25]	V_{lsr} km s^{-1}
28	IRAS 19075+1147	19 09 54.08	+11 52 47.7	-0.1493	-1.1405	4.8
29	IRAS 19076+1247	19 09 56.83	+12 52 56.5	-0.2791	-0.8719	47.4
30	IRAS 19081+0322	19 10 36.70	+03 27 02.3	-0.1017	-0.6345	41.5
31	IRAS19083+0851	19 10 47.33	+08 56 22.9	-0.466	-1.1792	45.5
32	IRAS 19085+0755	19 10 59.7	+08 00 23	-0.1117	-0.4708	76.1
33	IRAS 19112+0819	19 13 37.32	+08 24 52.4	-0.2219	-0.8206	38.6
34	IRAS 19128+0910	19 15 16.2	+09 15 46	-0.106	-0.9452	51.4
35	IRAS 19128+1310	19 15 07.97	+13 16 00.1	-0.2269	-0.9238	62.1
36	IRAS 19172+1956	19 19 28.7	+20 01 39	-0.2473	-0.8703	46.4
37	IRAS 19178+1206	19 20 14.01	+12 12 20.3	-0.0375	-0.6723	47.2
38	IRAS 19183+1148	19 20 42.59	+11 54 04.5	-0.0617	-0.7044	34.4
39	IRAS 19186+0315	19 21 11.70	+03 20 57.9	-0.3161	-1.2473	-22
40	IRAS 19188+1057	19 21 11.8	+11 02 49	-0.0898	-0.6306	-22.5
41	IRAS 19200+1035	19 22 26.67	+10 41 21.3	-0.1627	-0.663	53.4
42	IRAS 19200+1536	19 22 17.77	+15 41 49.0	-0.1587	-0.726	59.6
43	IRAS 19201+1040	19 22 29.2	+10 46 19	-0.2415	-0.9441	53.5
44	IRAS 19226+1401	19 24 54.1	+14 07 31	-0.1547	-0.554	4.7
45	IRAS 19248+1441	19 27 07.34	+14 47 21.7	-0.6179	-0.9149	36.8
46	IRAS 19254+1631	19 27 42.04	+16 37 24.0	0.0227	-0.5083	1.9
47	IRAS 19283+1944	19 30 29.48	+19 50 41.0	-1015	-0.72	27.4
48	IRAS 19295+2228	19 31 38.97	+22 35 17.2	-0.157	-1.2372	-74
49	IRAS 19316+0919	19 34 02.81	+09 26 06.2	-0.6692	-1.0971	76.4
50	IRAS 19343+2926	19 36 18.91	+29 32 50.0	0.1249	-0.1201	-0.9
51	IRAS19344+2457	19 36 32.03	+25 04 13.1	-0.1854	-1.1053	5.5
52	IRAS 19352+2030	19 37 24.00	+20 36 57.8	-0.0491	-0.776	-1.0
53	IRAS 19360+3442	19 37 57.77	+34 49 36.2	-0.2231	-1.075	-67.7
54	IRAS 19374+1626	19 39 40.4	+16 33 44	-0.0918	-0.7963	-29.5
55	IRAS 19440+2251	19 46 08.8	+22 59 24	-0.1574	-0.803	-7.5

Table 5.3 – Continued.

	IRAS Name	RA (J2000)	Dec (J2000)	[25-12]	[60-25]	V_{lsr} km s^{-1}
56	IRAS 19422+3506	19 44 07.00	+35 14 08.2	-0.4778	-1.2037	-48.4
57	IRAS 19425+3323	19 44 29.96	+33 30 38.4	-0.5992	-1.3373	9.6
58	IRAS 19451+1628	19 47 26.66	+16 35 35.9	-0.3762	-0.8812	25.4
59	IRAS 19462+2232	19 48 26.24	+22 39 56.8	-0.4705	-1.1791	13
60	IRAS 19520+2729	19 54 08.64	+27 37 01.8	-0.2232	-1.059	-1.3
61	IRAS 19565+3140	19 58 30.29	+31 48 16.1	-0.0472	-0.9063	20.4
62	IRAS 19575+1143	19 59 56.39	+11 51 45.1	-0.6458	-1.2636	-10.3
63	IRAS 19576+2814	19 59 39.14	+28 23 07.3	-0.0774	-0.8046	-58.7
64	IRAS 19579+3223	19 59 51.32	+32 32 09.8	-0.6494	-1.1285	5.5
65	IRAS 20023+2855	20 04 20.74	+29 04 06.5	0.0369	-0.5565	-64.8
66	IRAS 20043+2653	20 06 22.74	+27 02 10.6	-0.0378	-0.7358	-4.6
67	IRAS 20137+2838	20 15 47.65	+28 47 54.9	-0.088	-1.0455	-57.8
68	IRAS 20160+2734	20 18 05.886	+27 44 03.69	-1.002	-0.4328	6.1
69	IRAS 20267+2105	20 28 57.10	+21 15 37.0	-0.4063	-0.9582	-72.8
70	IRAS 20272+3535	20 29 08.4	+35 45 44	0.0502	-0.3928	-4.1
71	IRAS 20351+3450	20 37 07.95	+35 01 10.7	-0.5878	-1.2889	-5.4
72	IRAS 20403+3700	20 42 18.49	+37 11 41.0	-0.5545	-1.0878	-50.9
73	IRAS 20460+3253	20 48 03.36	+33 05 02.1	-0.6336	-1.1516	32
74	IRAS 20531+2909	20 55 17.8	+29 20 49	-0.17	-1.0648	-137

Table 5.4 – Results.

	IRAS Name	Engels & Lewis (1996)	Nov 2009	March 2011	April 2011
1	IRAS 18095+2704	N	N	N	N
2	IRAS 18341+0005	Y	N	N	N
3	IRAS 18349+1023	Y	Y	Y	Y
4	IRAS 18353+0020	N	N	N	N
5	IRAS 18395+0130	N	N	N	N
6	IRAS18398+1035	Y	Y	Y	Y
7	IRAS 18455+0448	N	Y	Y	Y
8	IRAS 18475+0353	N	N	N	N
9	IRAS 18490+0302	N	N	N	N
10	IRAS 18534+0215	N	N	N	N
11	IRAS 18549+0208	N	N	N	N
12	IRAS 18549+0905	Y	Y	Y	Y
13	IRAS 18568+0550	Y	N	N	N
14	IRAS 18571+0611	N	N	N	N
15	IRAS 18578+0831	Y	N	N	N
16	IRAS 18596+0315	Y	Y	Y	N
17	IRAS 19006+0624	N	N	N	N
18	IRAS 19012+1128	Y	N	Y	Y
19	IRAS 19017+0412	Y	N	N	N
20	IRAS 19017+0608	N	N	N	N
21	IRAS 19035+0451	Y	Y	Y	Y
22	IRAS 19043+1009	Y	N	N	N
23	IRAS 19052+0922	Y	N	N	N
24	IRAS 19054+0419	Y	N	N	N
25	IRAS 19065+0832	N	N	N	N
26	IRAS 19067+0811	Y	N	Y	Y
27	IRAS19069+0916	Y	Y	Y	Y
28	IRAS 19075+1147	N	N	N	N

Table 5.4 – Continued.

	IRAS Name	Engels & Lewis (1996)	Nov 2009	March 2011	April 2011
29	IRAS 19076+1247	N	N	N	N
30	IRAS 19081+0322	Y	Y	N	N
31	IRAS19083+0851	Y	Y	Y	Y
32	IRAS 19085+0755	Y	Y	Y	Y
33	IRAS 19112+0819	N	N	Y	Y
34	IRAS 19128+0910	N	N	N	N
35	IRAS 19128+1310	N	N	N	N
36	IRAS 19172+1956	N	N	N	N
37	IRAS 19178+1206	N	N	N	N
38	IRAS 19183+1148	N	N	N	N
39	IRAS 19186+0315	Y	Y	Y	Y
40	IRAS 19188+1057	N	N	N	N
41	IRAS 19200+1035	N	N	N	N
42	IRAS 19200+1536	N	N	N	N
43	IRAS 19201+1040	N	N	N	N
44	IRAS 19226+1401	N	N	N	N
45	IRAS 19248+1441	Y	Y	Y	Y
46	IRAS 19254+1631	N	Y	Y	Y
47	IRAS 19283+1944	N	N	N	N
48	IRAS 19295+2228	N	N	N	N
49	IRAS 19316+0919	Y	N	N	N
50	IRAS 19343+2926	N	N	N	N
51	IRAS19344+2457	N	N	N	N
52	IRAS 19352+2030	N	N	N	N
53	IRAS 19360+3442	N	N	N	N
54	IRAS 19374+1626	N	N	N	N
55	IRAS 19440+2251	N	N	N	N
56	IRAS 19422+3506	Y	Y	Y	Y
57	IRAS 19425+3323	Y	Y	N	N

Table 5.4 – Continued.

	IRAS Name	Engels & Lewis (1996)	Nov 2009	March 2011	April 2011
58	IRAS 19451+1628	Y	N	N	N
59	IRAS 19462+2232	Y	N	N	N
60	IRAS 19520+2729	N	N	N	N
61	IRAS 19565+3140	Y	Y	Y	Y
62	IRAS 19575+1143	Y	Y	Y	Y
63	IRAS 19576+2814	N	N	N	N
64	IRAS 19579+3223	Y	Y	Y	Y
65	IRAS 20023+2855	N	N	N	N
66	IRAS 20043+2653	N	N	N	N
67	IRAS 20137+2838	Y	Y	Y	Y
68	IRAS 20160+2734	N	N	N	N
69	IRAS 20267+2105	Y	Y	N	N
70	IRAS 20272+3535	N	N	N	N
71	IRAS 20351+3450	Y	Y	Y	Y
72	IRAS 20403+3700	Y	Y	Y	Y
73	IRAS 20460+3253	Y	Y	Y	Y
74	IRAS 20531+2909	N	N	N	N

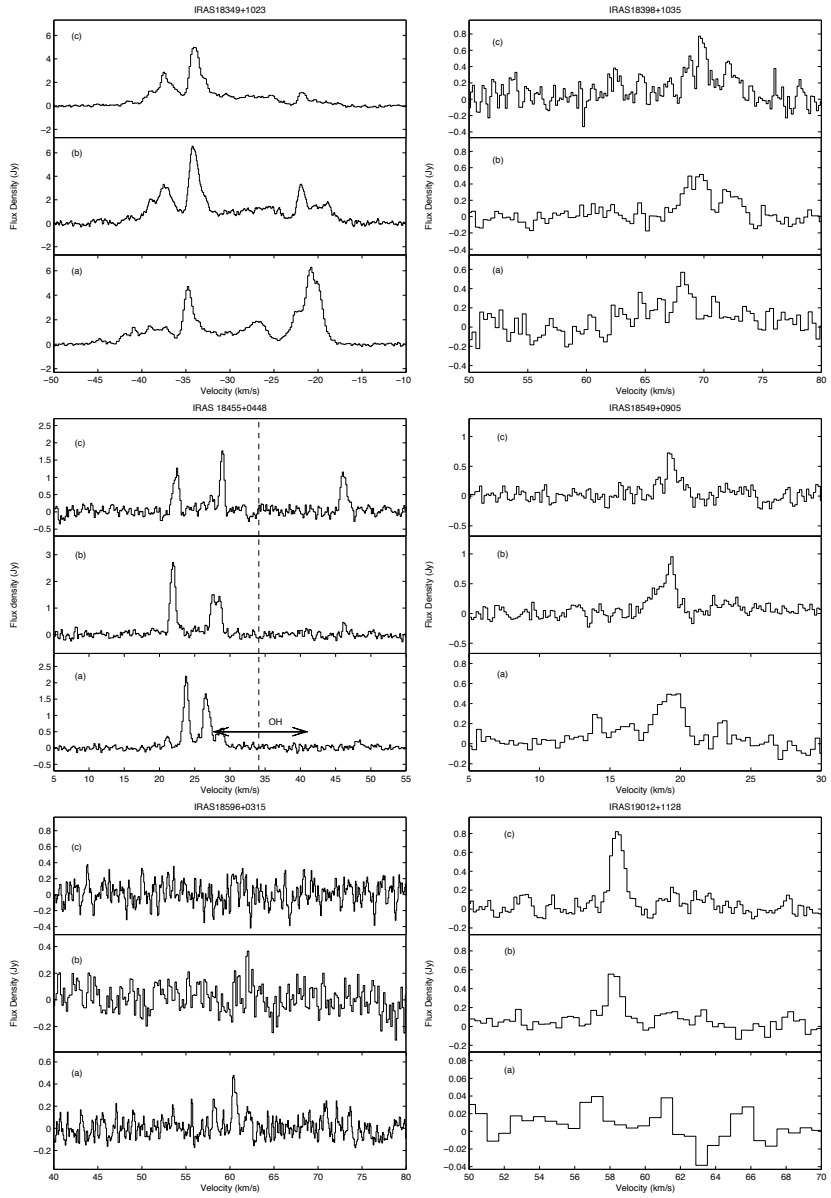

Figure 5.5 – H_2O maser spectra. Panels a, b and c show the spectrum observed at first (November 2009), second (March 2011) at third epochs (April 2011), respectively. The OH maser velocity range for water fountain candidates is shown in the plots. The dashed vertical lines indicate the stellar velocity.

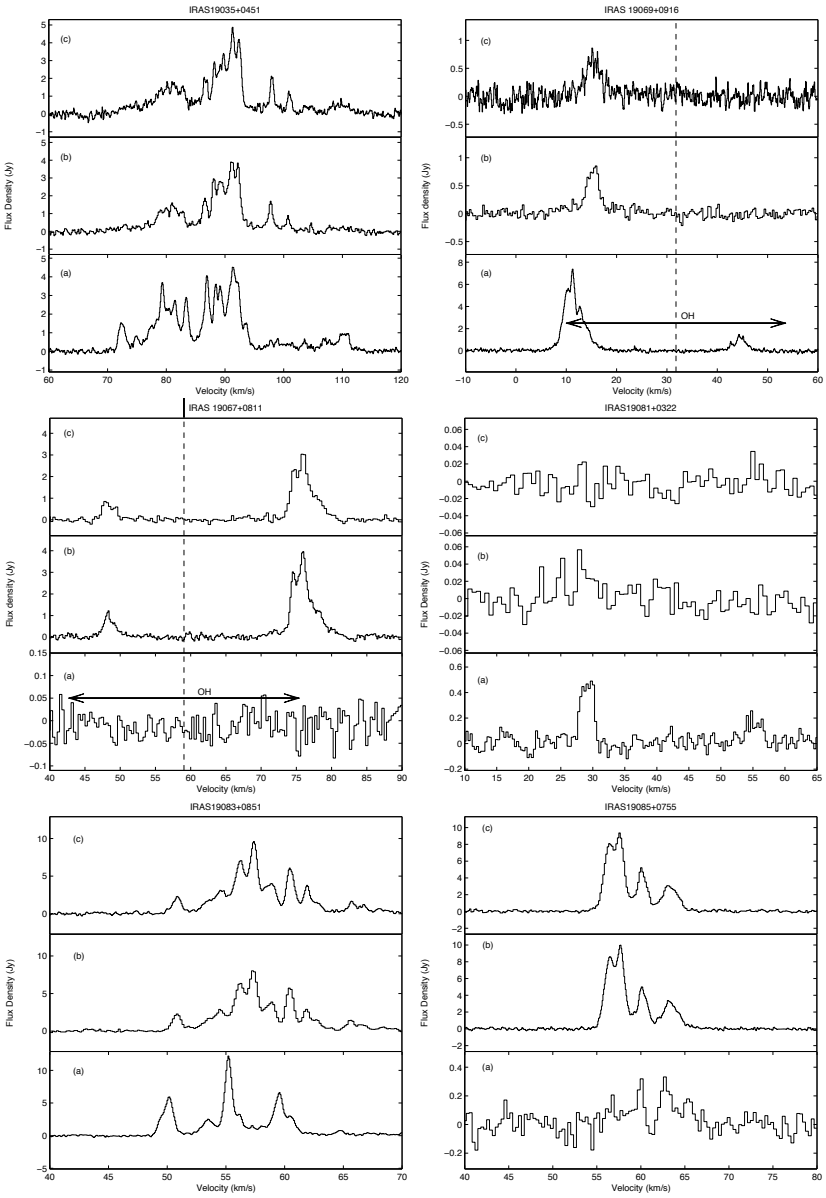

Figure 5.6 – Continued.

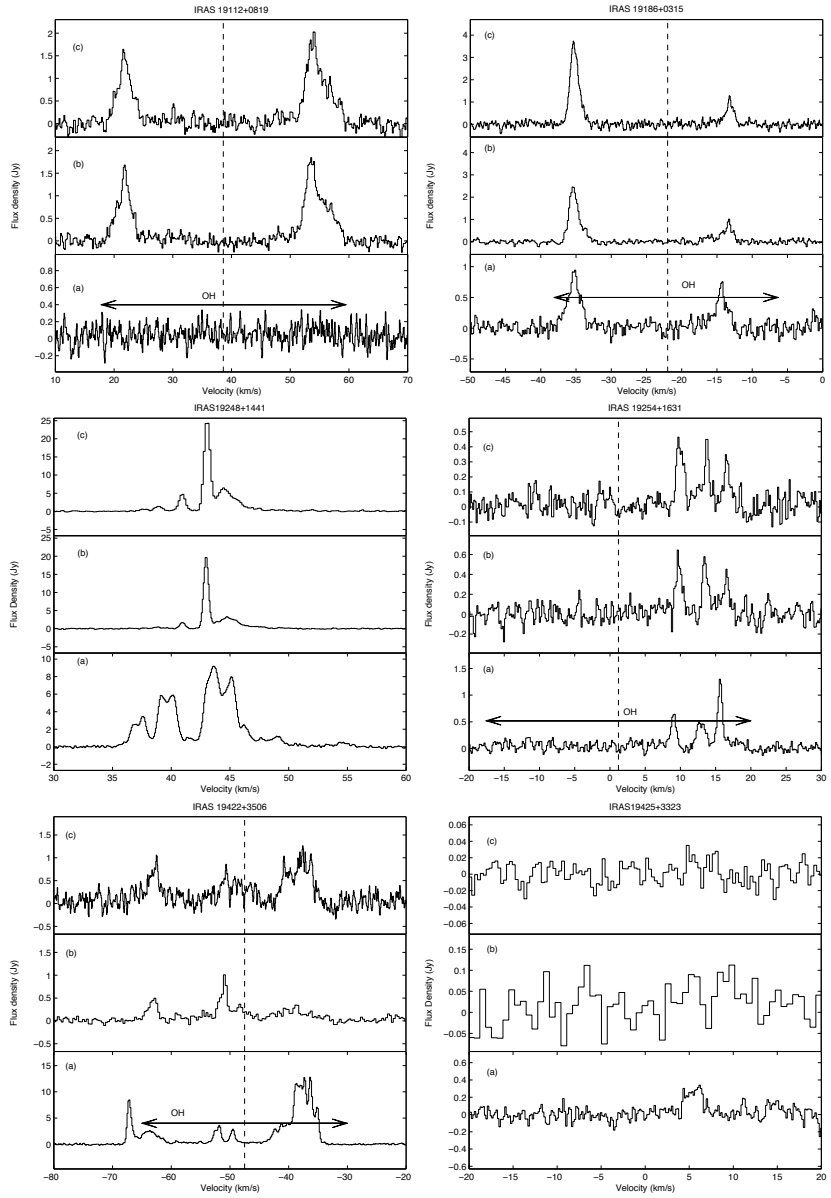

Figure 5.7 – Continued.

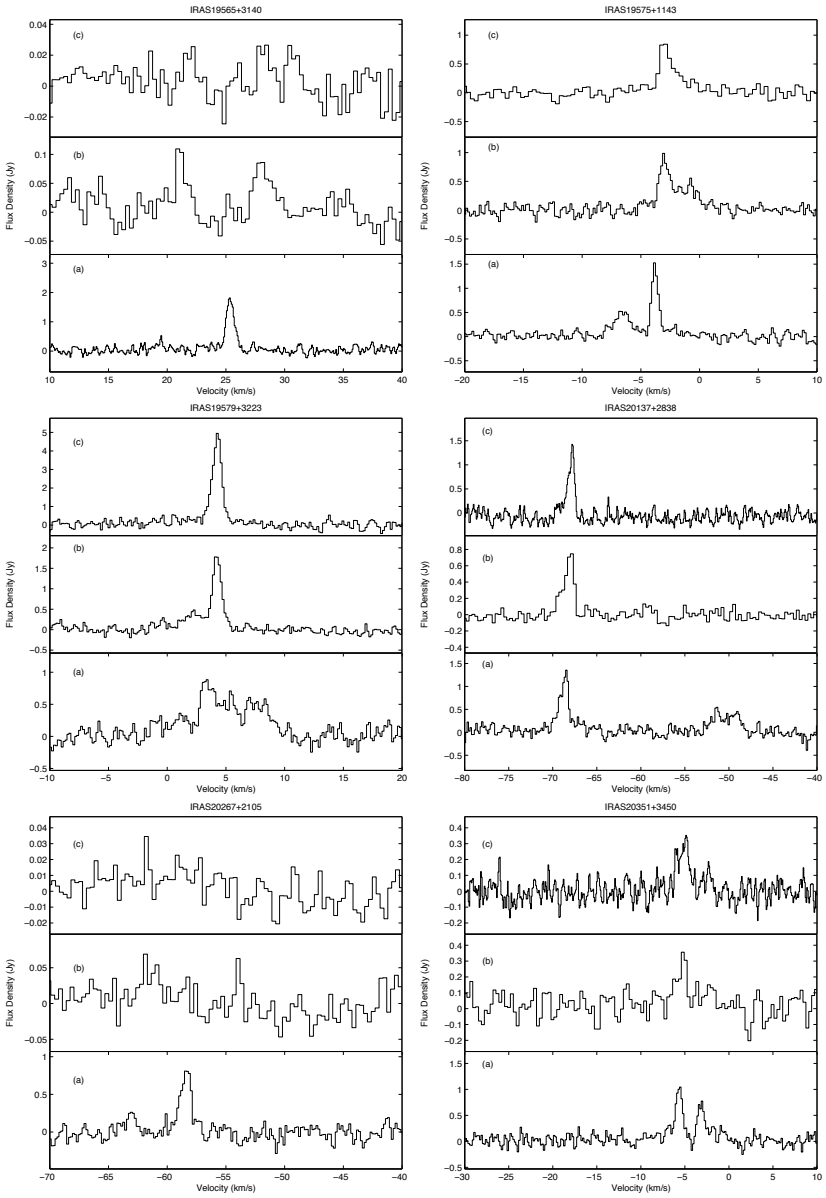

Figure 5.8 – Continued.

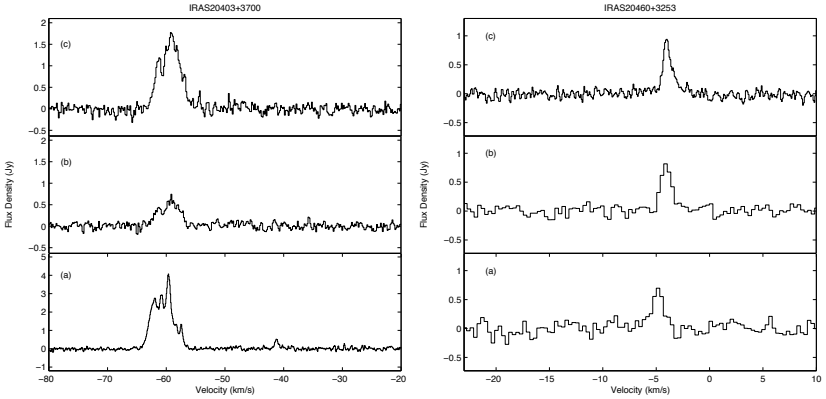

Figure 5.9 – Continued.